Published by IOP Publishing for Sissa Medialab

Received: *January 23, 2026*
Revised: *March 6, 2026*
Accepted: *March 12, 2026*
Published: *May 5, 2026*

Light Detection In Noble Elements (LIDINE 2025)
Hong Kong, China
21–24 October 2025

Impact of extreme ultraviolet radiation on the scintillation of pure and xenon-doped liquid argon

E. Nikoloudaki[a] **on behalf of the X-ArT collaboration**

[a] *APC, Université Paris Cité, CNRS, Astroparticule et Cosmologie, Paris F-75013, France*

E-mail: nikoloudaki@apc.in2p3.fr

Abstract: The X-ArT (Xenon-Argon Technology) collaboration has studied the scintillation mechanisms in pure and Xe-doped liquid argon (LAr) using silicon photomultipliers sensitive to different wavelength ranges. Thanks to these measurements we identified a long-lived (>10µs) component, compatible with extreme ultraviolet (EUV) photons emitted by the metastable levels of atomic argon. Based on this observation we developed a Xe-Ar scintillation model that includes both the EUV radiative contribution and the traditional collisional transfer process. Moreover we explored how the scintillation light yield and pulse shape discrimination vary as a function of the xenon concentration. Finally we proposed the EUV component as a possible source of the spurious electron emission in pure liquid argon, the main background in the search of light dark matter with noble liquid TPCs.

Keywords: Scintillators, scintillation and light emission processes (solid, gas and liquid scintillators); Noble liquid detectors (scintillation, ionization, double-phase); Dark Matter detectors (WIMPs, axions, etc.)

https://doi.org/10.1088/1748-0221/21/05/C05005

Contents

1 Introduction

Injecting just a few ppms of xenon in liquid argon [3, 4] is a cost effective way of combining the advantages of both elements, such as the strong pulse shape discrimination and lower energy thresholds of argon, as well as the sub-nanosecond timing resolution of xenon, due to its short decay states. The mixture operates close to the argon boiling point (87 K), that minimizes the dark count rate and xenon's wavelength (175 nm) is directly detectable by commercially available SiPMs. The applications of xenon-doped liquid argon span from solar neutrino physics and light dark matter searches, to neutrinoless double beta decay experiments [5] and positron emission tomography [6]. The X-ArT (Xenon-Argon Technology) collaboration has two main goals: to study the thermodynamic properties of the xenon-argon mixture and measure the maximum solubility of xenon in argon and to characterize the Ar-Xe response in scintillation and ionization up to the maximum xenon solubility. This document is based on the paper published in [1].

2 The X-ArT experimental setup

The experimental setup consists of a single-phase 4.5-cm diameter and 9.5-cm height cylindrical chamber equipped with silicon photomultipliers (SiPMs). The internal surfaces of the chamber are covered with an absorptive black foil to prevent reflections. No wavelength shifter is employed in the setup. 32 VUV-sensitive Hamamatsu S13371 SiPMs [9] are grouped in 8 channels at the top and bottom of the chamber. Half of the channels are covered with a quartz window that cuts wavelengths below 150 nm, while the windowless channels are sensitive to a broader range of wavelengths (figure 1).

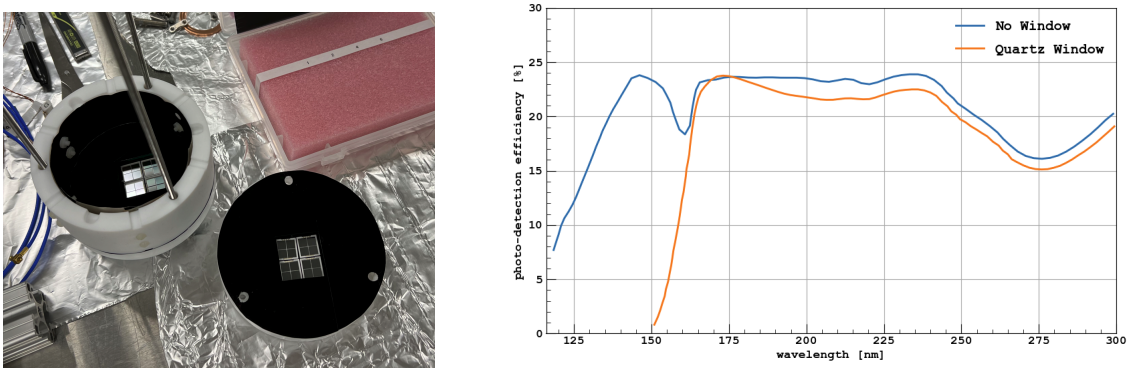

Figure 1. Left: An open view of the chamber. Right: Photo-detection efficiencies of the windowless (blue) and windowed (orange) channels. Reproduced from [1]. CC BY 4.0.

2026 JINST 21 C05005

3 EUV contribution in liquid argon

The data taking campaign began with a pure liquid argon run in order to constrain the triplet lifetime and assess the LAr purity. The LAr response model is defined as the convolution of the sum of the singlet and triplet state de-excitation times, the SiPM time-response, shown in figure 2, and the SiPM afterpulse time profile. The last two components were directly measured with laser calibrations. As seen in figure 2, the model is in good agreement with data up to 6 µs from the trigger. At longer times a discrepancy appears, which can be accounted for by adding an additional component with lifetime larger than 10 µs.

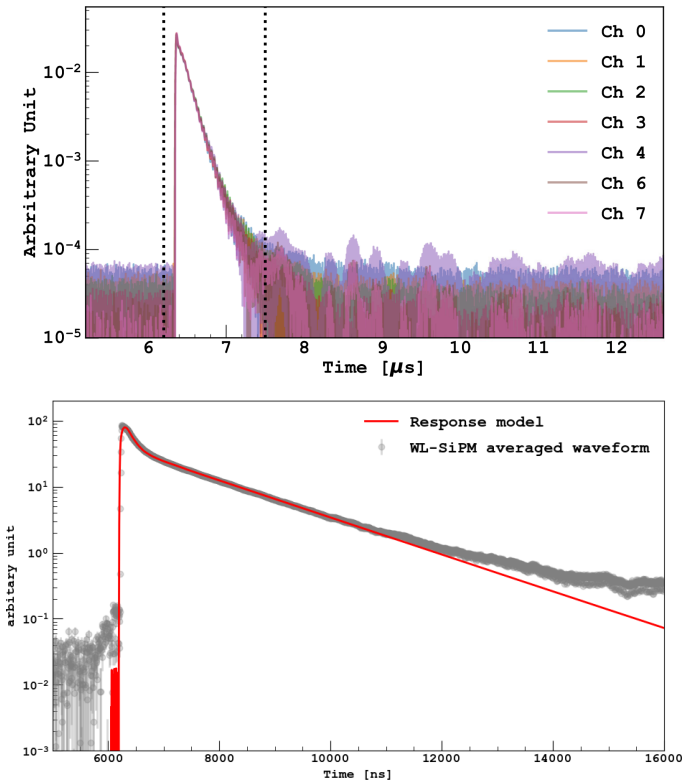

Figure 2. Top: SiPM time response. Bottom: Pure liquid argon scintillation averaged waveform, fitted with the liquid argon response model described in the text. Reproduced from [1]. CC BY 4.0.

This long component of liquid argon has been already observed in literature and assigned to the TPB wavelength shifter, PTFE fluorescence, or near-infrared photons [10–13]. However, there is no TPB in the X-ArT setup and all of the PTFE components have been covered with the absorptive foil. In addition, the near-infrared photon hypothesis can be ruled out since this component is detected only by SiPM without quartz, therefore at wavelengths below 150 nm.

It is known from atomic physics that neutral and singly or multiple ionized argon emits Extreme Ultraviolet (EUV) photons (10–100 nm) from metastable levels. The emission times range from ms to s, and EUV photons with wavelength lower than 100 nm (energy above 12.1 eV) can ionize Xe atoms [8]. This component has been detected by other setups, as reported in literature, since TPB is efficient in the EUV range as well [7]. In fact, this long tail in the pure liquid argon measurements, which we hypothesize is induced by EUV radiation, has been detected before, in setups that use PMTs and the TPB wavelength shifter, such as DEAP-3600 [2].

2026 JINST 21 C05005

4 The Xe-Ar scintillation model

The xenon-doped LAr scintillation model we developed consists of collisional and radiative branches, as shown schematically in figure 3. In the collisional branch where the energy transfer between argon and xenon is involved, there is a competition between the argon dimer de-excitation via 128-nm photons (τ_{128}) and collisions with a xenon atom and the subsequent ArXe* dimer formation with rate r_1. This dimer, in turn, can either decays via 150-nm photons (τ_{150} = 5 µs) or collisions with xenon to form a Xe_2^* dimer with rate r_3. The Xe_2^* decays instantaneously with its characteristic and very fast singlet and tripled decay times emitting 175-nm photons. In the radiative branch, EUV photons with wavelength smaller than 100 nm can directly ionize a xenon atom. The ionized xenon can then interact with argon and form an ArXe* excimer that follows the same path as in the collisional branch. The rate r_2 describes in total the radiative contribution, that is the EUV emission following the xenon ionization and ArXe* formation.

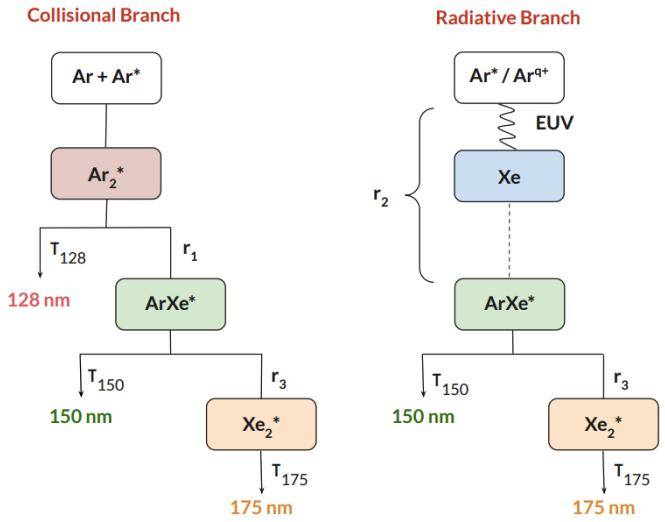

Figure 3. Model of xenon-argon scintillation. Reproduced from [1]. CC BY 4.0.

Data were acquired with ^{60}Co and ^{22}Na radioactive sources by triggering both windowed and windowless channels at the same time. Averaged waveforms were obtained by selecting a total number of photoelectrons between 300 and 700 across all channels to avoid saturation. Two data campaigns were carried out, one for xenon concentrations between 0.1 ppm and 2.7 ppm and one between 2.7 ppm and 40 ppm. A combined fit of waveforms from windowed and windowless channels allows to disentangle the contribution of the different wavelength components. From figure 4 it is evident that there is a non-zero contribution of the radiative branch and that the collisional process alone, cannot explain the data.

Figure 5 is obtained by averaging the fit results once Xe concentration reaches the stability after each Xe injection. At low xenon doping, argon is most likely to de-excitation via Ar_2^* as it is unable to collisionally transfer energy to a xenon atom. The radiative process does not depend on the xenon concentration but on the formation of atomic and ionized argon excited states that emit in the EUV, in a regime where photons can ionize xenon. The mean EUV-xenon scattering length is negligible compared to the size of the X-ArT chamber, so the increase of xenon concentration does not impact on the r_2 rate.

2026 JINST 21 C05005

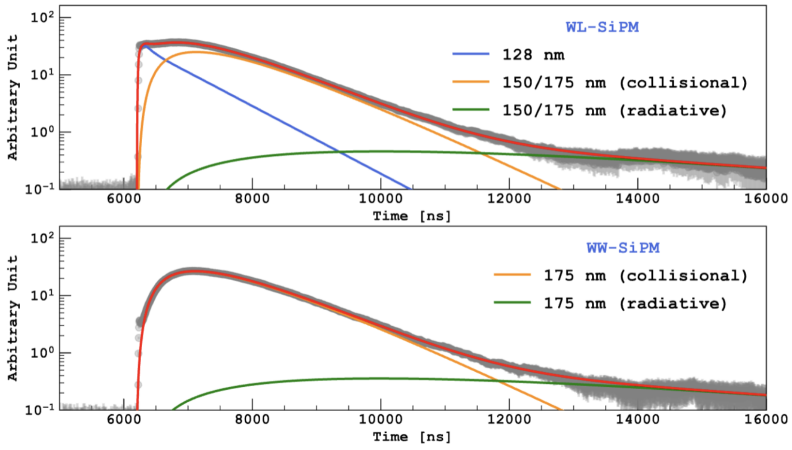

Figure 4. Simultaneous fit of the WW- and WL- channel averaged waveforms at 2.7 ppm xenon concentration using a ^{60}Co source. Reproduced from [1]. CC BY 4.0.

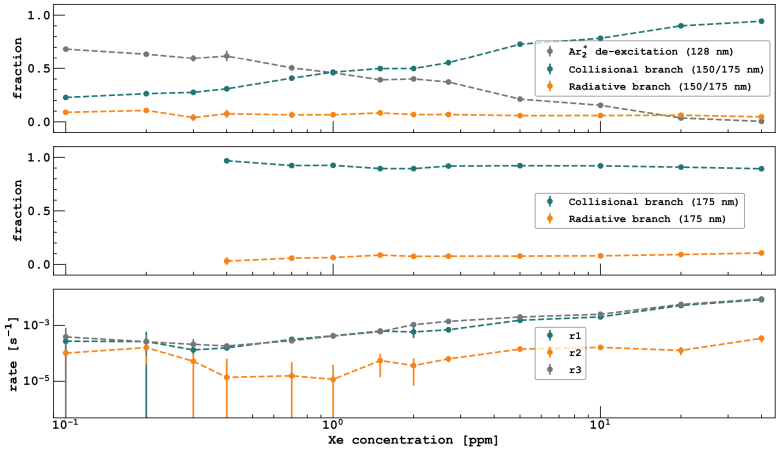

Figure 5. Fit parameter evolution as a function of the xenon concentration. The fraction refers to the relative contribution of each process. Reproduced from [1]. CC BY 4.0.

The first effect of xenon doping is a 15% increase of the light yield due to the additional ArXe* formation in the radiative branch, as can be seen in figure 6. As the channels with quartz window (WW-channels) detect only the light from xenon, the relative light yield, compared to the light yield at 0 ppm from the windowless SiPMs, increases with the xenon doping because of the increase of Xe_2^* decays. Above 20 ppm of xenon, the contribution to the light yield due to Xe_2^* becomes more important than the contribution from Ar_2^*. At 40 ppm the WW-light yield is about 6% less than the windowless channel (WL) light yield. For the WL-channels the relative light yield increases very fast at just a few ppm of xenon which implies that the ArXe* light contribution is much stronger than the Ar_2^* one. The radiative hypothesis well explain the 15% increase observed already at very low xenon concentration.

Xenon doping also affects the pulse shape discrimination (PSD), a parameter crucial for background rejection in dark matter experiments with liquid argon. The PSD observable (w) is here defined as the fraction of light detected by the WL-channels in the first 300 ns. Electron and nuclear recoil samples are produced by exposing the chamber to ^{22}Na and ^{241}AmBe sources, respectively. To study the

2026 JINST 21 C05005

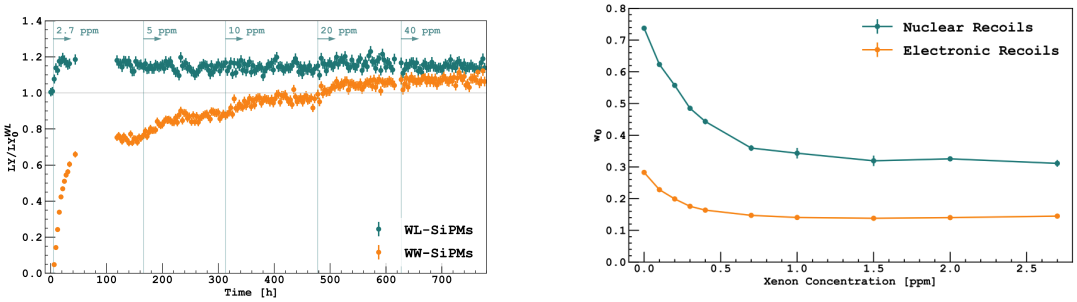

Figure 6. Left: Relative light yield fit results at different xenon injection times for the WL- and WW-channels. The vertical lines indicate the amount of xenon injected into the system. Right: PSD distribution centroids as a function of the xenon concentration for electron and nuclear recoils. Reproduced from [1]. CC BY 4.0.

effect of xenon doping on the PSD, the fitted centroids w_0 of the w distributions of the electron and nuclear recoils are compared in figure 6. With increasing xenon doping, the electron and nuclear recoil centroid difference decreases and stabilizes after around 1 ppm. However these results are directly affected by the limited photo-detection efficiency of the current setup.

Lastly, the EUV hypothesis is a compelling explanation of the spurious electrons (SE), electroluminescence pulses of unknown origin, equivalent to one or few electrons that are correlated with preceding events and impurities. This represents the main background in the search for light dark matter in both liquid argon and xenon experiments. Their origin is hypothesized to be electrons trapped by impurities and released with a time delay or delayed electron extraction from the grid of the TPC. Atomic argon EUV photons are able to ionize trace impurities in liquid argon, since their energy is higher that the impurities' ionization threshold [14]. This hypothesis is consistent with the energy correlation, since more energetic events lead to more atomic argon excitation and with the time correlation because of the millisecond to fraction of seconds emission times of atomic argon metastable levels.

References

[1] X-ArT collaboration, *Impact of extreme ultraviolet radiation on the scintillation of pure and xenon-doped liquid argon*, *Phys. Rev. D* **111** (2025) 102001 [arXiv:2410.22863].

[2] DEAP collaboration, *The liquid-argon scintillation pulseshape in DEAP-3600*, *Eur. Phys. J. C* **80** (2020) 303 [arXiv:2001.09855].

[3] C. Vogl et al., *Scintillation and optical properties of xenon-doped liquid argon*, 2022 *JINST* **17** C01031 [arXiv:2112.07427].

[4] C. Galbiati et al., *Pulse shape study of the fast scintillation light emitted from xenon-doped liquid argon using silicon photomultipliers*, 2021 *JINST* **16** P02015 [arXiv:2009.06238].

[5] A. Mastbaum, F. Psihas and J. Zennamo, *Xenon-doped liquid argon TPCs as a neutrinoless double beta decay platform*, *Phys. Rev. D* **106** (2022) 092002 [arXiv:2203.14700].

[6] A. Zabihi et al., *3Dπ: three-dimensional positron imaging, a novel total-body PET scanner using xenon-doped liquid argon scintillator*, *Phys. Med. Biol.* **70** (2025) 065015.

[7] C. Benson, G.D. Orebi Gann and V. Gehman, *Measurements of the intrinsic quantum efficiency and absorption length of tetraphenyl butadiene thin films in the vacuum ultraviolet regime*, *Eur. Phys. J. C* **78** (2018) 329.

2026 JINST 21 C05005

[8] J.M. Ajello, G.K. James, B. Franklin and S. Howell, *Study of electron impact excitation of argon in the extreme ultraviolet: emission cross section of resonance lines of Ar I, Ar II*, *J. Phys. B* **23** (1990) 4355.

[9] Hamamatsu, *Si photodiode S1337 series*, https://www.hamamatsu.com/eu/en/product/optical-sensors/photodiodes/si-photodiodes/S1337-1010BQ.html,.

[10] J. Asaadi et al., *Emanation and bulk fluorescence in liquid argon from tetraphenyl butadiene wavelength shifting coatings*, 2019 *JINST* **14** P02021 [arXiv:1804.00011].

[11] R. Jerry, L. Winslow, L. Bugel and J.M. Conrad, *A Study of the Fluorescence Response of Tetraphenyl-Butadiene*, arXiv:1001.4214.

[12] NEXT collaboration, *Reflectance and fluorescence characteristics of PTFE coated with TPB at visible, UV, and VUV as a function of thickness*, 2023 *JINST* **18** P03016 [arXiv:2211.05024].

[13] T. Alexander, C.O. Escobar, W.H. Lippincott and P. Rubinov, *Near-infrared scintillation of liquid argon*, 2016 *JINST* **11** C03010 [arXiv:1603.02290].

[14] XENON100 collaboration, *Observation and applications of single-electron charge signals in the XENON100 experiment*, *J. Phys. G* **41** (2014) 035201 [arXiv:1311.1088].

2026 JINST 21 C05005